

Detection of extremely weak precipitation in Rikubetsu, inland Hokkaido, Japan

Naohiko HIRASAWA^{1,2} and Hiroyuki KONISHI³

¹ National Institute of Polar Research, Tachikawa, Tokyo, Japan

² Department of Polar Science, School of Multidisciplinary Sciences, SOKENDAI (The Graduate University for Advanced Studies), Tachikawa, Tokyo, Japan

³ Division of Math, Sciences, and Information Technology in Education, Osaka Kyoiku University, Osaka, Japan

(Received December 8, 2024; Revised manuscript accepted January 8, 2025)

Abstract

Due to the low temperature of the polar atmosphere, the amount of water vapor contained therein is low, and correspondingly, precipitation intensity is relatively weak. For example, in the interior of Antarctica, clear-sky precipitation accounts for half of the annual precipitation, and its contribution to the mass input of the Antarctic ice sheet is considered significant. However, no established method exists for continuously measuring such extremely weak precipitation in polar regions. This study examined how ceilometers, disdrometers, and precipitation weighing instruments can be applied to the detection of weak precipitation in Rikubetsu (43.5°N, 143.8°E), inland Hokkaido. The findings showed that the disdrometer and the ceilometer detected weak precipitation even when precipitation-weighing instruments did not. This precipitation was classified as extremely weak precipitation Type-I (EWP-I) when it had a relatively high precipitation intensity, and as Type-II (EWP-II) when it had a lower intensity. EWP-II was detected by the disdrometer, which detects precipitation particles, and by the ceilometer, which measures backscatter intensity. During EWP-II events, actual precipitation particles were discernable and could be photographed. EWP-II events are observed mainly under ice-saturated conditions at night, when there is an increase in relative humidity due to the decrease in surface air temperature associated with radiative cooling. The ceilometer observed increases in backscatter relatively soon after the temperature drop began after daytime maxima were recorded. Since the disdrometer cannot detect particles smaller than 125 μm , the ceilometer might be better suited to capturing the effects of smaller particles. Weaker precipitation detected only by the ceilometer was classified as extremely weak precipitation of Type-III (EWP-III). The detection of EWP-II and EWP-III demonstrates the potential for recording the occurrence of extremely weak precipitation, including clear-sky precipitation, in polar regions.

Key words: snowfall, precipitation, ceilometer, disdrometer, weighing gauge, Double Fence Intercomparison Reference (DFIR), Rikubetsu

1. Introduction

In polar and cold regions, the total precipitation is lower, and precipitation intensity is weaker compared to other regions, reflecting the low temperatures in these regions. For example, precipitation over the Antarctic region ranges from a few tens of millimeters a day in coastal area to a few millimeters per day inland, even during relatively heavy precipitation events associated with synoptic-scale disturbances (e.g., Konishi et al., 1998, Schlosser et al., 2010).

Even today, accurately measuring snowfall is challenging. The World Meteorological Organization (WMO), along with national weather agencies, researchers, and engineers, are engaged in various experiments and observations to address this issue. Recently, the WMO conducted an international project titled “Solid Precipitation Intercomparison Experiment (SPICE)” during the winters of 2013–2016 (e.g., Nitu et

al., 2018, Qiu, 2012). This was the third attempt of its kind, following similar projects in the past. We participated in the most recent SPICE project using data collected at our observation site in Rikubetsu, northern Japan (Hirasawa et al., 2018).

Snowfall outside polar and extremely cold regions is relatively heavy and intense. For such snowfall, the main concerns for accurate measurements are improving the capture rate of precipitation particles and minimizing evaporation losses after collection. These were the central issues addressed during SPICE. In contrast, polar precipitation is characterized by a higher proportion of extremely weak-intensity precipitation events, reflecting the extremely low temperatures in other regions. This adds the additional challenge of measuring precipitation at such low intensities, in addition to the problems associated with accurately measuring capture rate and evaporation. For example, if daily precipitation of 1 mm

occurs over 24 hours of continuous precipitation, the precipitation intensity would be 0.04 mm/hr. According to Hirasawa *et al.* (2018), this value is comparable to the resolution of Geonor T200B, one of the standard weighing gauges.

In Antarctica, relatively large precipitation events associated with synoptic-scale disturbances occur only a few times per year, with a maximum frequency of about 10 times annually (Schlosser *et al.*, 2010, Turner *et al.*, 2019). Another major precipitation system in Antarctica is clear-sky precipitation, commonly referred to as diamond dust. Clear-sky precipitation has been recognized as a significant contributor to mass input for the Antarctic ice sheet, not based on quantitative measurements, but because it occurs up to 80% of the year in the interior region (e.g., King and Turner, 1997). Annual precipitation at the coastal Syowa Station is approximately 200 mm (Konishi *et al.*, 1998), while in inland areas along the traverse route between Syowa Station and Dome Fuji, it is about 30 mm (Motoyama *et al.*, 2015). If half of the annual precipitation is attributed to clear-sky precipitation and it occurs over 180 days (i.e., half of the year), then the daily precipitation rate would be 0.56 mm/day (0.02 mm/hr) at Syowa Station and 0.08 mm/day (0.003 mm/hr) in inland areas. These values indicate that the resolution of Geonor T200B is insufficient for measuring clear-sky precipitation on an hourly basis.

Lidars and laser disdrometers can detect very weak precipitation. Gorodetskaya *et al.* (2015) showed that a ceilometer detected very weak snowfall or ice cloud layer below 1000 m from ground surface at Princess Elisabeth Station in coastal Antarctica. But converting these measurements into precipitation amounts presents challenges. Lolli *et al.* (2018) examined methods for estimating precipitation intensity for very weak rainfall (<3 mm/hr) using micropulse lidar and disdrometer observations. Rocadenbosch *et al.* (2020) proposed a method to estimate precipitation intensity from backscatter measurements obtained using a Vaisala CL31 ceilometer during rain events with intensities below approximately 10 mm/hr. The backscattering intensity of the laser is influenced not only by the quantity of particles, but also by the shape of the ice crystals and the orientation of their faces when the scatterers are ice particles. Consequently, efforts to estimate precipitation intensity from laser backscatter intensity have focused primarily on rainfall. An effort targeting ice particles involved the development of an algorithm to detect the presence or absence of blowing snow using a ceilometer (Gossart *et al.*, 2017).

Based on the Clausius-Clapeyron equation, global warming is expected to promote an increase in water vapor, leading to an increase in precipitation. Trenberth *et al.* (2003) estimated that the rate of increase in atmospheric water vapor capacity is approximately 7%

K^{-1} , which implies that the overall rate of the increase in precipitation should follow the same trend. In the latest Intergovernmental Panel on Climate Change (IPCC) special report (Meredith *et al.* 2019; The Ice sheet Mass Balance Inter-comparison Exercise (IMBIE) Team 2018), it is projected that Antarctic precipitation will increase as warming progresses.

This increase in precipitation is attributed to both relatively intense precipitation events associated with synoptic disturbances, which can be measured by radar (Hirasawa *et al.* 2022), and extremely weak precipitation, such as clear-sky precipitation. Accurately quantifying the amount and intensity of weak precipitation, including clear-sky precipitation, remains challenging when using lidars, ceilometers, and laser disdrometers. However, these instruments can, to some extent, detect the presence or absence of weak precipitation. Detecting and recording the intensity and duration of weak precipitation in Antarctica would be valuable, as such records serve as indicators of global warming and could be used effectively in future studies.

In this study, we investigated the effectiveness of a ceilometer and a laser disdrometer for detecting extremely weak precipitation and compared these findings to measurements obtained using conventional precipitation measurement methods. The data for the analysis were obtained in Rikubetsu, one of the coldest regions in Japan (Sorai *et al.*, 2016), where clear-sky precipitation is occasionally observed.

2. Observations and analysis

2.1 Observation site and instruments

Snowfall and meteorological measurements have been conducted at an observation site in Rikubetsu (43.5°N, 143.8°E, 217 m above sea level) since 2012 (Fig. 1a). Rikubetsu is located on the eastern side of the central mountain range in Hokkaido (indicated by the white dashed line in Fig. 1a). During heavy snowfall events on the Sea of Japan side of Hokkaido caused by the Asian winter monsoon, most of the areas on the Pacific Ocean side, including Rikubetsu, generally experience clear skies. Snowfall in Rikubetsu is typically associated with frontal activity driven by synoptic-scale disturbances passing through the region (e.g., Kawase *et al.*, 2023, Hirasawa and Konishi, 2024). The daily winter minimum air temperature occasionally drops below -30°C. This cold environment makes Rikubetsu a valuable test site for conducting snowfall observations relevant to Arctic and Antarctic conditions.

The specifications of the instruments used in this study are summarized in Table 1, and the location of each instrument is shown in Fig. 1b. The backscatter coefficients measured by the ceilometer (Fig. 1c) and the particle counts recorded by the disdrometer (Fig. 1d) allowed the detection of extremely weak precipitation events that were not captured by the two weighing

gauges installed at the site. The disdrometer was placed at the center of a wooden double-fence enclosure designed for wind protection.

One of the weighing gauges (Fig. 1e), manufactured by Geonor Inc. (Norway), is an internationally recognized standard instrument. It was positioned at the center of another wooden double fence. During SPICE, data from this Geonor weighing gauge data were used for intercomparison among observation sites as part of the Double Fence Intercomparison Reference (DFIR). The second weighing gauge was custom-built, consisting of a bucket and an electronic scale (Fig. 2a). It was designed to achieve higher sensitivity than the Geonor weighing gauge, making it suitable for detecting relatively weak precipitation events. However, it was less reliable for measuring precipitation amounts due to sublimation from the snow surface in the bucket and the relatively low catchment rate of snow particles. This latter limitation was attributable to a simple windshield constructed from plastic nets.

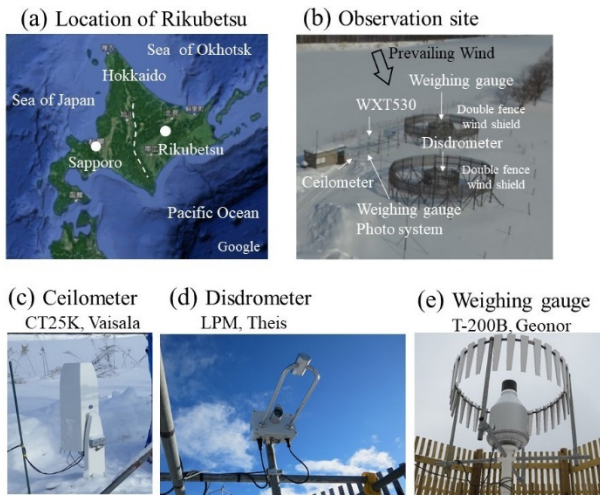


Fig. 1 (a) Map of Hokkaido showing Rikubetsu and topography of the region; (b) Landscape surrounding the observation site; (c) Ceilometer; (d) Disdrometer in the double fence windshield; and (e) Weighing gauge in the double fence windshield.

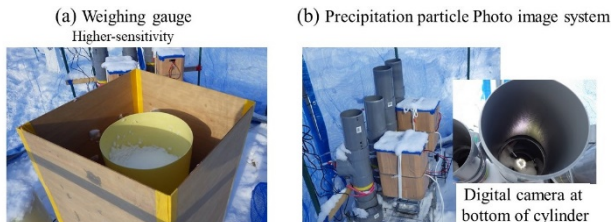


Fig. 2 (a) Weighing gauge with higher-sensitivity; (b) Precipitation particle imaging system.

An automatic photography system was installed (Fig. 2b). The system consisted of a digital camera positioned

in the lower part of a plastic cylinder. The camera captured images of the surface of a plastic plate from below at one-minute intervals.

Table 1 Specifications of instruments for precipitation measurements

Instrument	Model name, Manufacturer, Country
Description	
Ceilometer	CT25K, Vaisala, Finland
Backscatter coefficient of a laser with a wave length of 905 nm	
Every 30 m layer from the ground level to a height of 7500 m	
Data interval: 15 seconds	
Observation period: December 1, 2014 - March 31, 2015	
Disdrometer	LPM, Thies Clima, Germany
Number of particles per minute by particle size and fall velocity	
Small particle size classification: 0-125 μm , 125-250, 250-375, 375-500, 500-750, 750-1000	
Precipitation intensity (mm/hr) determined from laser attenuation	
Data interval: 1 minute	
Observation period: December 1, 2014 - March 31, 2015	
Weighing gauge	T-200B, Geonor Inc., Norway
Cumulative precipitation (mm)	
Resolution: 0.02-0.05 mm, depending on the weight	
Data interval: 1 minute	
Observation period: December 1, 2014 - March 31, 2015	
Weighing gauge	Custom-built for higher sensitivity measurement
Cumulative precipitation (mm)	
Resolution: 0.001 mm (bucket diameter: 365 mm, weight resolution: 0.1 g)	
Data interval: 15 seconds	
Observation period: December 23, 2014 - February 14, 2015	
Precipitation particle photography	Custom-built
Digital image	
Data interval: 1 minute with cleaning up by air splayed	
Observation period: December 22, 2014 - January 1, 2015, January 11 - 15, 2015	
Surface Meteorology-1	WXT530, Vaisala, Finland
Temperature, wind speed and direction, relative humidity, pressure	
Data interval: 15 seconds	
Observation period: December 1, 2014 - January 1, 2015, January 16 - 24, 2015, February 1 - 7, 2015, February 19 - March 31, 2015	
Surface Meteorology-2	Custom-built in conjunction with manufacturers
Temperature (Platinum Resistance), relative humidity (HMP45D, Vaisala, Finland)	
Data interval: 1 hour	
Observation period: December 1, 2014 - March 31, 2015	

Surface meteorological observations were conducted using two sets of instrumentation. Surface Meteorology-1 (Table 1) was installed near the snowfall instruments (Fig. 1b). However, due to frequent data gaps, measurements from Surface Meteorology-2 (Table 2), located approximately 50 m away, were also used in the analysis. To address differences in air temperature and relative humidity measured by the two instruments, the data from Surface Meteorology-2 were corrected to match those from instrument 1. Let T1, RH1, T2, RH2,

T_{2c} , and RH_{2c} represent the air temperature and relative humidity recorded by instrument 1, instrument 2, and after correction, respectively. The following correction equations, obtained through linear regression, were applied: $T_{2c} = 0.9778 T_2 + 0.9568$, $RH_{2c} = 0.7401 RH_2 + 16.606$.

2.2 Analysis

The ceilometer recorded backscatter coefficients at intervals of 30 m from the ground level to a height of 7500 m. For this study, backscatter coefficients from the first and second lowermost layers, corresponding to altitudes of 0–30 m and 30–60 m, were analyzed. It should be noted that the lowermost layer may be contaminated by snow particles lofted from the ground surface under the strong wind conditions, and we need to handle this possibility with that in mind, and this possibility was considered during the analysis.

The disdrometer measured precipitation intensity based on laser attenuation and recorded the size distribution of precipitation particles. Particle size (diameter) was classified into the following size ranges: 0–125 μm , 125–250 μm , 250–375 μm , 375–500 μm , 500–750 μm , 750–1000 μm , and larger size classes. Due to frequent errors of unknown origin in the smallest class (Hirasawa et al. 2018), data from this size class were excluded from the analysis.

During extremely weak precipitation events, the disdrometer often recorded a precipitation intensity of 0 mm/hr while detecting particles within the smaller diameter range. Therefore, we analyzed the number of particles with diameters between 125 and 1000 μm as evidence for the occurrence of extremely weak precipitation.

The Geonor weighing gauge, with a resolution of approximately 0.04 mm, was also used. However, it has been reported that its measurements are subject to drift caused by diurnal variations in temperature (Hirasawa et al., 2018). For example, a temperature change of 20°C can result in a change as large as 5 mm, which is equivalent to 10 times the instrument's resolution.

In the remainder of the paper, we first examine whether precipitation events weaker than the detection threshold of the Geonor weighing gauge can be detected by other instruments. Next, we identify the most effective measurements for detecting extremely weak precipitation events. Finally, we discuss the possible formation mechanism of these extremely weak precipitation events.

3. Results

3.1 Detection of precipitation events

Figure 3 shows the time series of precipitation intensity (mm/10 min) and cumulative precipitation (mm) measured by three instruments. The Geonor weighing gauge (Fig. 3a) exhibits diurnal variations with an

amplitude of approximately ± 0.05 mm/10 min, caused by temperature-dependent drift in the measured values. These diurnal variations are compensated for in the cumulative precipitation data. Values greater than +0.05 mm, as detected by the Geonor weighing gauge, are considered precipitation events and are shaded red in all panels of Fig. 3.

The higher-sensitivity weighing gauge (Fig. 3b) detected precipitation events weaker than 0.05 mm/10 min outside the red-shaded periods. Unlike the Geonor weighing gauge, this weighing gauge did not suppress sublimation from the snow surface, which primarily resulted in negative precipitation intensity during the daytime. The cumulative precipitation shown here represents the cumulative precipitation minus sublimation, reflecting the water balance at the snow cover surface. It is important to note that this measurement may underestimate or fail to detect precipitation when sublimation and precipitation occur simultaneously during the daytime. The comparison of precipitation intensity between the higher-sensitivity weighing gauge and the Geonor weighing gauge (Fig. 4a) may reflect this underestimation. Precipitation events outside the red-shaded periods in Figure 3 correspond to the datapoints plotted to the left of the red vertical line in Figure 4.

The disdrometer (Fig. 3c) also detected precipitation events weaker than 0.05 mm/10 min, with their timing closely matching that of the higher-sensitivity weighing gauge. The cumulative precipitation measured by the disdrometer was the largest among the three instruments. This is likely because, unlike the higher-sensitivity weighing gauge, the disdrometer is not affected by snow sublimation. However, further validation of precipitation intensity estimates based on laser attenuation should be conducted in the future. As shown in Fig. 4b, the disdrometer tended to overestimate precipitation intensity compared to the Geonor weighing gauge more frequently than the higher-sensitivity weighing gauge. However, verification of the quantitative accuracy of these measurements lies outside the scope of this study.

3.2 Extremely weak precipitation events

Figure 4 shows that in almost all cases where the Geonor weighing gauge detected precipitation, the disdrometer also detected precipitation (Fig. 4b). Conversely, there are several instances where precipitation detected by the Geonor weighing gauge was not detected by the higher-sensitivity weighing gauge (circled in Fig. 4a), likely due to sublimation. Therefore, this study defines the very weak precipitation events that were detected by the laser attenuation method of the disdrometer, that is, more than 0 mm/10 min, during periods when the Geonor weighing gauge did not detect precipitation as Extremely Weak Precipitation of Type-I (EWP-I) events.

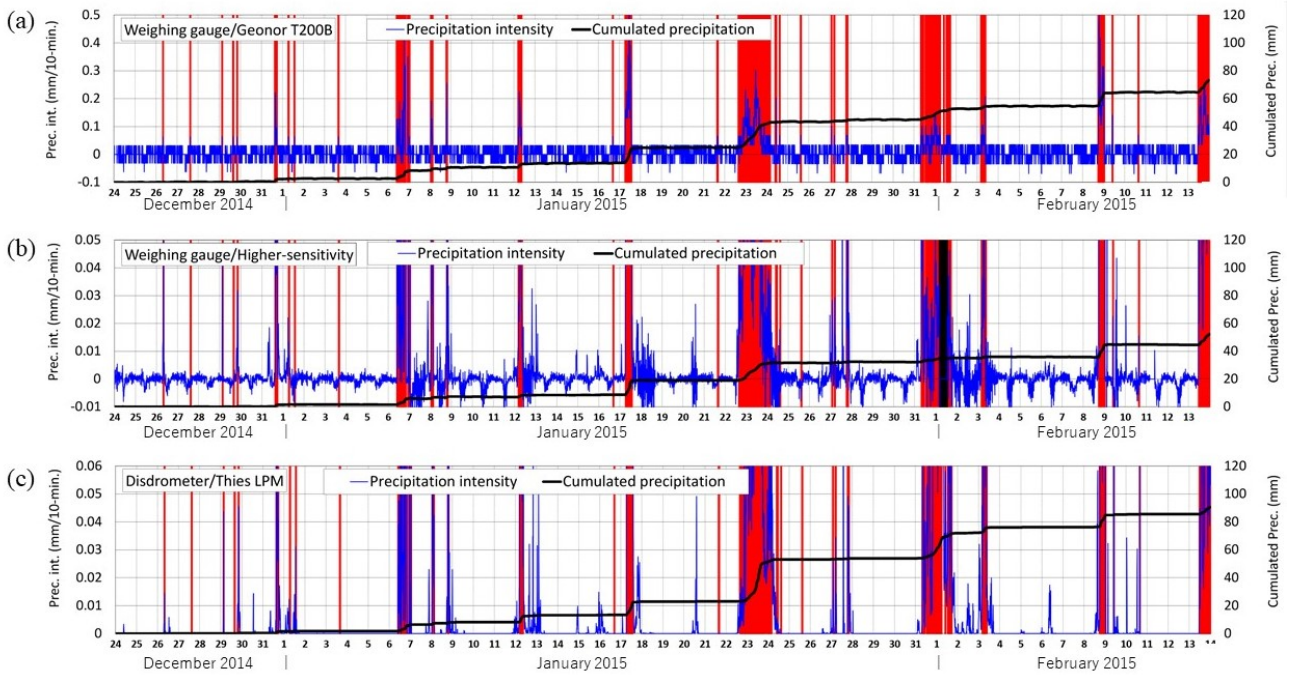


Fig. 3 Time series of precipitation intensity (mm/10 min) and cumulative precipitation (mm) from December 24, 2014 to February 13, 2015 for (a) the Geonor weighing gauge, (b) the higher-sensitivity weighing gauge (with approximately eight hours of data missing on February 1, indicated by black shading), and (c) the disdrometer. Periods when the Geonor weighing gauge detected precipitation exceeding 0.05 mm in 10 minutes are indicated by red shading.

Figure 5 shows a time series of particle counts per minute for particles with diameters ranging from 125 to 1000 μm , measured over 10-minute intervals by the disdrometer, alongside the averaged backscatter coefficients for the two lowermost layers measured over 10-minute intervals by the ceilometer. Periods identified as EWP-I are shaded in green.

The disdrometer recorded particle counts even outside the EWP-I periods. Particles in the smaller size range of 125 to 1000 μm were detected primarily during the nighttime. This diurnal variability was not identified in the study by Hirasawa and Konishi (2023), which analyzed diurnal variability at this station, including the period of this study, because their analysis excluded precipitation that occurred outside the EWP-I periods.

Variability in the backscatter coefficients for the lowermost layer (0–30 m in height) measured by the ceilometer correlates with the particle counts recorded by the disdrometer. In certain cases, indicated by the bold downward-pointing arrow in Fig. 5a), precipitation particles were captured in photographs, as shown in Fig. 6. This suggests that the observed variability in particle counts and backscatter coefficients likely reflects actual precipitation. Diurnal variability is also evident in the second lowermost layer of the ceilometer but is notably suppressed overall, e.g., on December 28 and January 4–5. This suppression in the upper layer may be related to the mechanism of precipitation particle formation, which

will be discussed in the following section.

This paper defines the extremely weak precipitation detected based on the particle counts of the disdrometer or the backscatter intensity of the ceilometer, occurring outside the EWP-I periods, as Extremely Weak Precipitation of Type-II (EWP-II).

4. Discussion

4.1 Temporal occurrence of extremely weak precipitation

Table 2 summarizes the temporal occurrence of each type of precipitation event. The analysis period consisted of 7498 ten-minute intervals, during which the Geonor weighing gauge detected precipitation in 469 intervals. This represents the normally observed precipitation, indicating an overall precipitation incidence of 6.3% during this study period.

EWP-I was detected in 1493 of the remaining 7020 10-minute intervals, excluding periods when the Geonor weighing gauge detected precipitation. This corresponds to 20% of the total time. Similarly, EWP-II detected by either instrument occurred in 1802 of the remaining 5527 ten-minute intervals, accounting for approximately one-third of the time. This significant temporal occurrence of EWP-II is comparable to clear-sky precipitation in Antarctica.

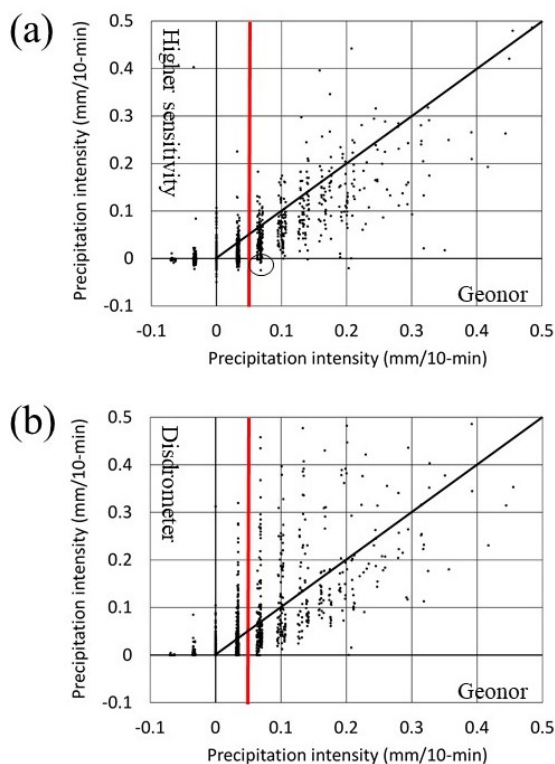


Fig. 4 Comparison of measured precipitation intensity between instruments. (a) Geonor weighing gauge vs. higher-sensitivity weighing gauge; (b) Geonor weighing gauge vs. disdrometer. Precipitation events detected by the Geonor weighing gauge are plotted to the right of the red vertical line (0.05 mm/10 min). The circle in (a) indicates the reference area discussed in the text.

4.2 Diurnal variability of EWP-II

Figure 7 shows the time dependence of the EWP-II. Precipitation particles in the smallest diameter range were frequently detected between 21:00 and 6:00 JST. During this period, stronger backscatter intensity ($\geq 5 \times 10^{-7} \text{ sr}^{-1} \text{ m}^{-1}$) was detected by the ceilometer more frequently than at other times of the day. This paper refers to this backscatter intensity as an indicator of precipitation particles.

The contrast between nighttime and daytime for EWP-II is more pronounced for particle detection data from the disdrometer than in the ceilometer backscatter intensity (Fig. 7b). Specifically, from December 24 to January 5, nighttime particle detection by the disdrometer exceeded the mean value by a factor of two, while it decreased to a factor of 0.2 during the daytime. The ceilometer backscatter intensity also exhibited a distinct nighttime-to-daytime contrast during the same period. Notably, the increase in backscatter intensity toward nighttime began around 18:00, earlier than the rise in particle counts detected by the disdrometer.

The contrast between nighttime and daytime backscatter intensities was considerably weaker during

the analyzed period. One possible explanation for this is that the backscatter intensity of the ceilometer is affected by changes in the amount of scatterers other than precipitation particles. This factor should be considered when detecting EWP-II using the backscatter intensity of the ceilometer.

4.3 Mechanism of the EWP-II formation at night

Figure 8 compares the time series of backscatter intensity and particle counts with surface air temperature and relative humidity (with respect to ice) from December 24, 2014, to January 5, 2015. Surface temperatures ranged between -5°C during the daytime and -25 to -30°C at night. Relative humidity exceeded 100% at around 17:00 to 18:00 when the temperature was dropping, and it remained below 100% by approximately 9:00 when the temperature increased markedly. The occurrence of EWP-II, indicated by increases in both backscatter intensity and particle detection, appears to be related to the development of low-temperature and high-humidity conditions at night. Relative humidity with respect to ice often remained below 100%, suggesting that the precipitation particles that formed during this period were ice crystals, commonly referred to as diamond dust.

The mechanism responsible for the formation of EWP-II, as well as the differences in variation between ceilometer backscatter intensity and disdrometer particle detection, are analyzed using altitude-time cross-sections of the ceilometer backscatter coefficient (Fig. 9) and detailed time series of temperature and relative humidity (Fig. 10).

Figure 9 shows precipitation from the upper atmospheric levels on December 26, from 7:00 to 14:00, and on December 29, from 3:00 to 4:00 and after 18:00. During these periods, EWP-I and EWP-II co-occurred (Fig. 5). In contrast, from the evening of December 26 to the morning of December 28, EWP-II events did not originate as precipitation from upper atmospheric levels. On both nights, the atmosphere became ice-saturated before 18:00 and remained so until after 8:00 the following morning. The disdrometer detected precipitation particles only under these ice-saturated conditions, while water saturation was not reached during either night (data not shown). These observations suggest that the EWP-II events during these nights were likely associated with the deposition of ice crystals, which subsequently fell.

Conversely, the backscatter intensity of the ceilometer increased at approximately 15:00 before the onset of ice saturation. This timing closely followed the decrease in temperature from the daytime maximum and likely reflected the growth of hygroscopic aerosols. These observations suggest that EWP-II was composed of supercooled water droplets, at least during the starting phase.

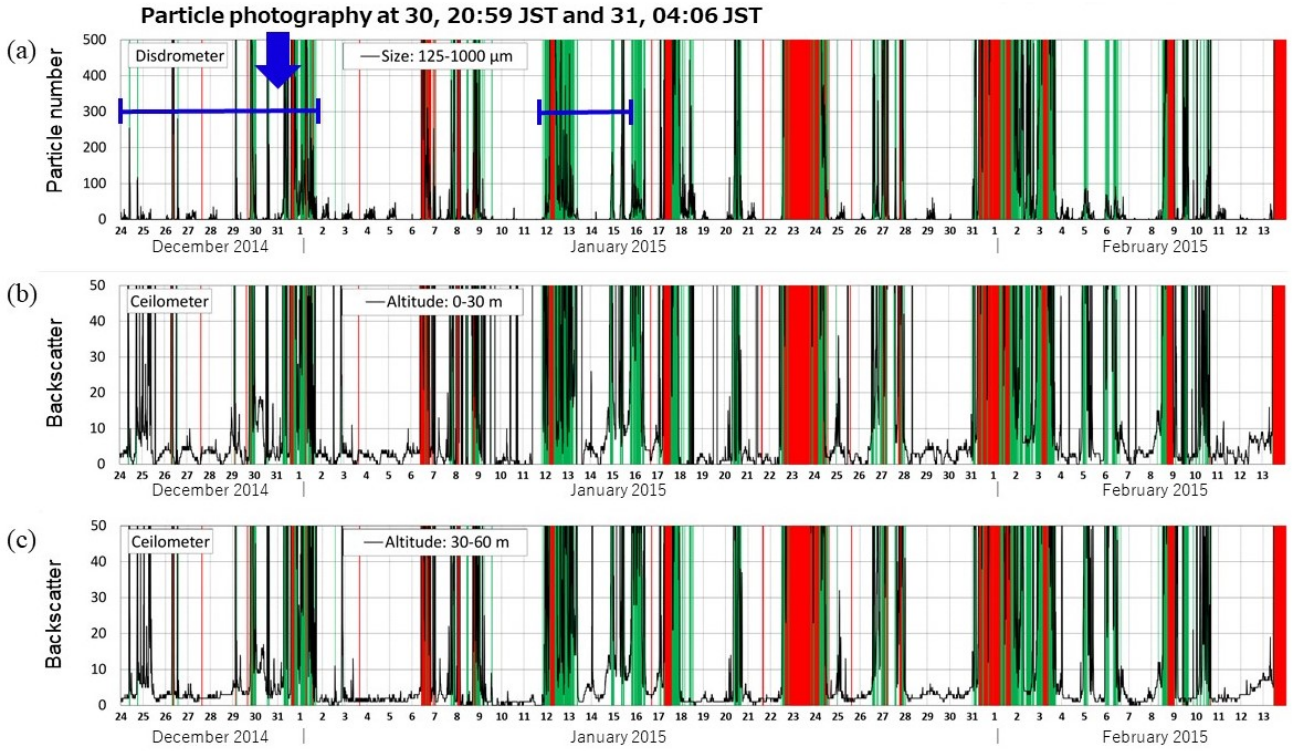


Fig. 5 Time series of precipitation-related measurements. (a) Averaged number of particles (per minute) with diameters ranging from 125 to 1000 μm , measured over 10-minute intervals by the disdrometer, and (b, c) averaged backscatter coefficients of the atmospheric layers at heights of 0–30 m and 30–60 m, respectively, measured over 10-minute intervals by the ceilometer. Periods of EWP-I are shaded in green. In (a), blue lines with whiskers indicate the periods during which precipitation particle photography was conducted. The blue arrow marks the timing of the precipitation photographs shown in Fig. 6.

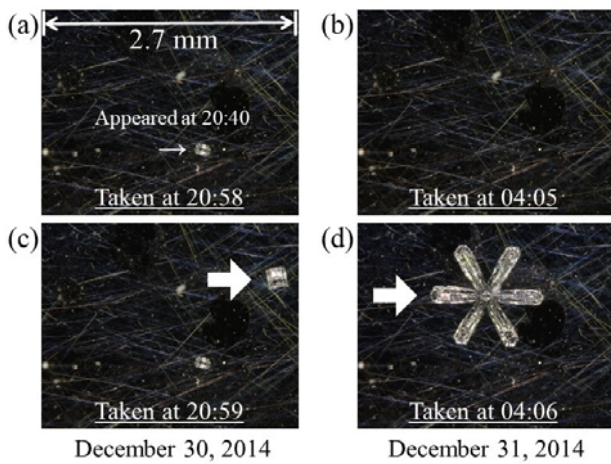


Fig. 6 Sequential precipitation particle photographs taken during EWP-II. Photographs captured at (a) 20:58 (JST) and (c) 20:59 on December 30, 2024, and at (b) 04:05 and (d) 04:06 on December 31, 2024. Bold arrows indicate particles that appeared within the 1-minute interval. The smaller arrow indicates a particle that appeared previously, with the corresponding time. The horizontal width of each photograph is 2.7 mm.

Table 2 Temporal occurrence of each type of precipitation

Instruments, Data Items	Precipitation	Extremely weak precipitation of Type-I	Extremely weak precipitation of Type-II
	Time Detected / Total Eligible Time (10-minute intervals) Percentage (%)		
Geonor weighing gauge	469 / 7489 6.3%	-	-
Disdrometer (attenuation)	-	1493 / 7020 21.3%	-
Disdrometer (particle counts) 125 μm - 1 mm	-	-	1730 ^(*) / 5527 31.3%
Ceilometer (backscatter) ($\geq 5 \times 10^{-7} \text{ sr}^{-1} \text{ m}^{-1}$) Layer 0-30 m in height	-	-	1802 ^(*) / 5527 32.6%

*Note: 855 times were synchronized

However, in all cases, the EWP-II observed during the two nights could have been formed by radiative cooling of the ground surface. While the disdrometer only detects particles larger than 125 μm , the ceilometer may have observed backscattering from smaller particles, suggesting that the ceilometer backscatter intensity could potentially be a more effective method for detecting extremely weak precipitation in colder polar regions.

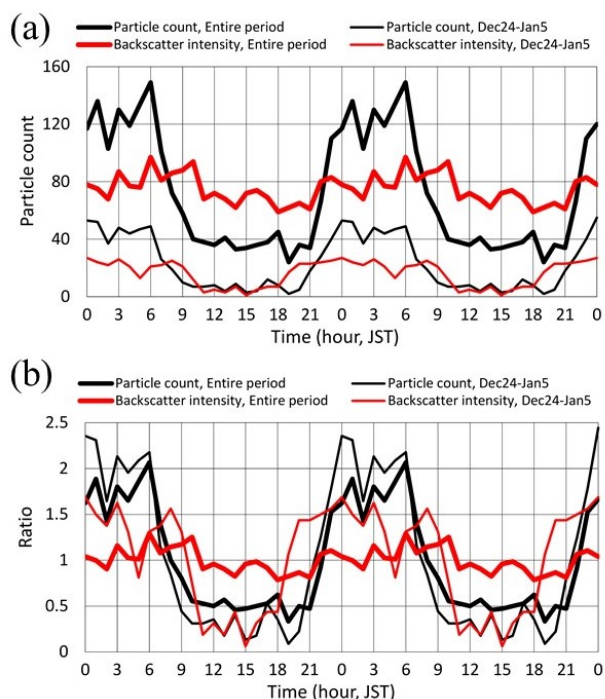


Fig. 7 Time dependence of EWP-II. (a) Black lines represent the 10-minute counts during which the disdrometer detected particles, while the red lines represent the 10-minute counts during which the ceilometer backscatter intensity was $\geq 5 \times 10^{-7} \text{ sr}^{-1} \text{ m}^{-1}$ in the 0–30 m layer. Thick lines indicate the entire analyzed period, while thin lines represent data from December 24 to January 5, when the diurnal variation is clearly characterized. The 24-hour cycle is shown repeated twice. (b) Same as (a), but showing the ratio to the mean.

The promotion of particle formation and growth may be weaker in the second lowermost layer, from 30 m to 60 m in height, than in the first layer because of the smaller temperature drop induced by radiative cooling of the ground surface. In addition, particles fall out into the first layer. These processes cause the variation in ceilometer backscatter to be less in the second layer than in the first layer.

From the evening of December 28 to the morning of December 29, the minimum temperature appeared around 0:00 on December 29, which differs from the pattern observed on the previous two nights. Ice saturation was only observed briefly, before and after the minimum temperature occurred. The backscatter intensity recorded by the ceilometer began to increase after the daytime maximum temperature and reached higher values at around 0:00, which coincided with the minimum temperature. Unlike the preceding two nights, this increase in backscatter at midnight was associated with precipitation from upper clouds. The disdrometer detected precipitation particles only once, at 0:10. These observations suggest that the ceilometer is better suited

for detecting extremely weak precipitation, particularly of small particles, than the disdrometer. Precipitation detected solely by the ceilometer may be classified as Extremely Weak Precipitation of Type-III (EWP-III).

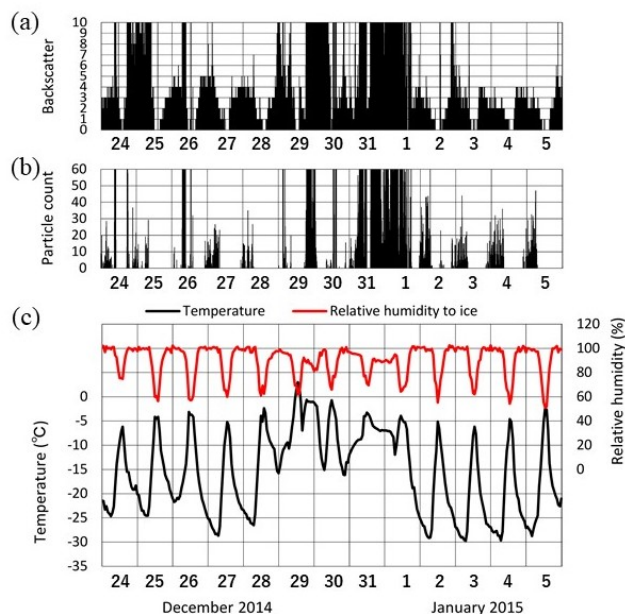


Fig. 8 Time series data. (a) Backscatter intensity ($10^{-7} \text{ sr}^{-1} \text{ m}^{-1}$) in the 0–30 m layer, (b) particle counts for diameters ranging from 125 to 1000 μm in diameter, and (c) temperature and relative humidity with respect to ice, as observed by the Surface Meteorology-2, from December 24, 2014, to January 5, 2015.

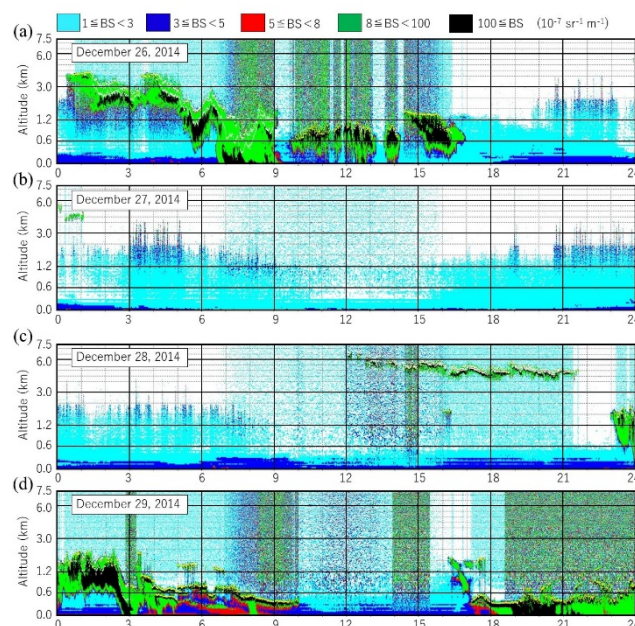


Fig. 9 Altitude-time cross-section of backscatter coefficient measured by the ceilometer from December 24 to 29, 2014.

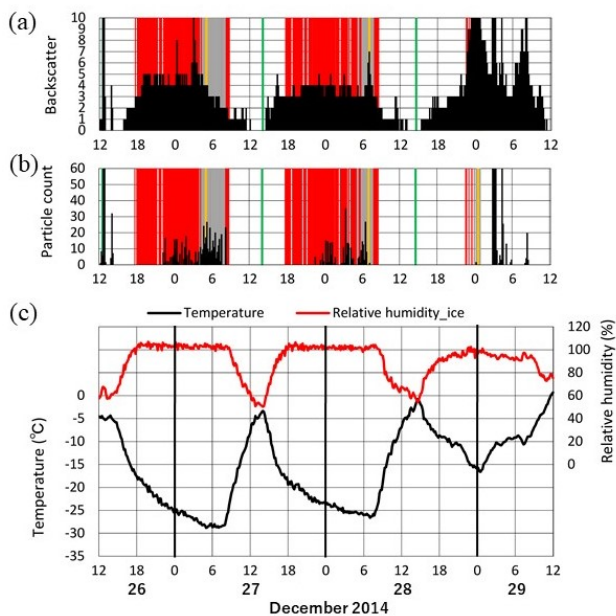


Fig. 10 Same as Fig. 8, but with observations from Surface Meteorology-1 from 12:00, December 26 to 12:00, December 28, 2014. In (a) and (b), red shading indicates periods of ice saturation, while gray shades mark times within 1°C of the nighttime minimum temperature (vertical orange line). The vertical green line represents the time of the daytime maximum temperature.

The precipitation particles detected by the disdrometer in non-ice-saturated conditions on the morning of December 29 are presumed to have originated from upper clouds.

5. Conclusion

Measuring extremely weak precipitation in polar regions is crucial due to the low temperatures and corresponding low humidity in these areas. Understanding the contribution of such precipitation, including clear-sky precipitation, to the ice mass balance of the Antarctic ice sheet is essential for understanding the mechanisms of ice sheet mass change related to global warming and for improving future projections using climate models. However, no established method currently exists for measuring such weak precipitation in polar regions. This study examined how ceilometers, disdrometers, and precipitation weighing instruments detect weak precipitation in Rikubetsu (43.5°N, 143.8°E), inland Hokkaido. The findings showed that the disdrometer and ceilometer detected weak precipitation that was not recorded below the detection thresholds of precipitation weighing measurements. Weak precipitation was classified into Extremely Weak Precipitation of Type-I (EWP-I), characterized by relatively high precipitation intensity, and Extremely Weak Precipitation of Type-II (EWP-II), characterized

by lower intensity. EWP-II was detected by the disdrometer, which detects precipitation particles, and by the ceilometer, which measures backscatter intensity. During EWP-II events, actual precipitation particles were photographed. EWP-II occurred mainly at night, where the increase in relative humidity caused by surface air temperature drops due to radiative cooling was a key factor. The disdrometer detected precipitation particles only under ice-saturated conditions, while the ceilometer recorded increases in backscatter relatively soon after temperatures began to decline following daytime maximums. Since the disdrometer could not detect particles smaller than 125 μm , the ceilometer likely captured the effects of smaller particles. Precipitation detected only by the ceilometer is classified as Extremely Weak Precipitation of Type-III (EWP-III). The identification of EWP-II and EWP-III highlights the potential of using ceilometers and disdrometers to record extremely weak precipitation, including clear-sky precipitation, in polar regions.

Acknowledgements

The observations described in this study were conducted as part of a scientific project administered by the National Institute of Polar Research (NIPR) through Project Research No. KP-302. This study was supported by the 3rd Research Announcement on the Earth Observations (EORA3) program administered by the Japan Aerospace Exploration Agency (JAXA). Surface Meteorology-2 data was obtained with the assistance of the Institute for Research and Development in Technology of Cold Regions, based in Rikubetsu. The authors thank FORTE Science Communications (<https://www.forte-science.co.jp/>) for English language editing.

References

- Gorodetskaya, I. V. and 8 co-authors (2015): Cloud and precipitation properties from ground-based remote-sensing instruments in East Antarctica. *The Cryosphere*, 9(1), 285–304. <https://doi.org/10.5194/tc-9-285-2015>
- Gossart, A. and 8 co-authors (2017): Blowing snow detection from ground-based ceilometers: application to East Antarctica. *The Cryosphere*, 11(6), 2755–2772. <https://doi.org/10.5194/tc-11-2755-2017>
- Hirasawa, N. and 3 co-authors and project group of Japan Meteorological Agency (2018): SPICE site report: Rikubetsu, Japan. WMO Solid Precipitation Intercomparison Experiment (SPICE), *Instruments and Observing Methods*, 131, Annex 8.3, December 2018.
- Hirasawa, N. and 4 co-authors (2022): Snowfall detection by a newly deployed X-band Doppler radar at Syowa Station, Antarctica. *Okhotsk Sea and Polar Oceans Research*, 6, 36–41. <https://doi.org/10.57287/ospor.6.36>
- Hirasawa, N. and H. Konishi (2023): Diurnal variation in precipitation and cloud formation during winter in Rikubetsu, inland Hokkaido, northern Japan. *Okhotsk Sea and Polar Oceans Research*, 7, 30–35. <https://doi.org/10.57287/ospor.7.30>

- Hirasawa, N. and H. Konishi (2024): Intra-seasonal and inter-annual variations in snowfall and rainfall during winter in Rikubetsu, inland Hokkaido, Japan. *Okhotsk Sea and Polar Oceans Research*, **8**, 1-6. <https://doi.org/10.57287/ospo.8.1>
- Kawase, H., and 7 co-authors (2023): Historical regional climate changes in Japan in winter as assessed by a 5-km regional climate model with a land surface process. *Prog. Earth Planet. Sci.*, **10**(1), 7. <https://doi.org/10.1186/s40645-023-00536-4>
- King, J. C., and Turner, J. (1997): *Antarctic Meteorology and Climatology*. Cambridge: Cambridge University Press. <https://doi.org/10.1017/CBO9780511524967>
- Konishi, H., Wada, M., and Endoh, T. (1998): Seasonal variations of cloud and precipitation at Syowa station, Antarctica. *Annals of Glaciology*, **27**, 597–602. <https://doi.org/10.3189/1998AoG27-1-597-602>
- Lolli, S. and 15 co-authors (2018): Vertically Resolved Precipitation Intensity Retrieved through a Synergy between the Ground-Based NASA MPLNET Lidar Network Measurements, Surface Disdrometer Datasets and an Analytical Model Solution. *Remote Sensing*, **10**(7), 1102. <https://doi.org/10.3390/rs10071102>
- Meredith, M. and 12 co-authors (2019): Polar Regions, In *IPCC Special Report on the Ocean and Cryosphere in a Changing Climate* [Pörtner, H.-O. and 12 co-authors (eds.)]. https://www.ipcc.ch/site/assets/uploads/sites/3/2019/11/07_SROCC_Ch03_FINAL.pdf
- Motoyama, H. and 25 co-authors (2015): Glaciological Data Collected by the 48th–54th Japanese Antarctic Research Expeditions during 2007–2013. *JARE Data Reports. Glaciology*, **35**, 1–44. <https://doi.org/10.15094/00010905>
- Nitu, R., and 42 co-authors (2018): WMO Solid Precipitation Intercomparison Experiment (SPICE). *Instruments and Observing Methods*, **131**. <https://library.wmo.int/opac/>
- Qiu, J. (2012). Snow survey hopes for avalanche of data. *Nature*, **491**, 312-313. <https://doi.org/10.1038/491312a>
- Rocadenbosch, F. and 6 co-authors (2020): Ceilometer-Based Rain-Rate Estimation: A Case-Study Comparison With S-Band Radar and Disdrometer Retrievals in the Context of VORTEX-SE. *IEEE Transactions on Geoscience and Remote Sensing*, **58**(12), 8268–8284. <https://doi.org/10.1109/TGRS.2020.2984458>
- Schlosser, E., and 5 co-authors (2010): An extreme precipitation event in Dronning Maud Land, Antarctica: a case study with the Antarctic Mesoscale Prediction System. *Polar Research*, **29**(3), 330–344. <https://doi.org/10.3402/polar.v29i3.6072>
- Sorai, T., H. Hamada, T. Kameda, and S. Takahashi (2016): Rikubetsu, the coldest town in Japan: according to the meteorological data by Japan Meteorological Agency from 2007 to 2016 in winter seasons. *Tenki*, **63**, 879-887. (in Japanese)
- The IMBIE team (2018): Mass balance of the Antarctic Ice Sheet from 1992 to 2017, *Nature* **558**, 219-222. <http://doi:10.1038/s41586-018-0179-y>
- Turner, J. and 12 co-authors (2019). The Dominant Role of Extreme Precipitation Events in Antarctic Snowfall Variability. *Geophysical Research Letters*, **46**(6), 3502–3511. <https://doi.org/10.1029/2018GL081517>

Summary in Japanese

和文要約

北海道内陸部の陸別における 極端に弱い降雪の検出

平沢尚彦^{1,2}, 小西啓之³

¹ 国立極地研究所, ² 総合研究大学院大学, ³ 大阪教育大学

極域の大気は低温のために、そこに含まれる水蒸気量は少なく、それに応じて降水強度が比較的弱い。例えば南極内陸では晴天降水が年間の半分以上の時間を占めることから、南極氷床の涵養にとって晴天降水の寄与の大きさが想像されてきた。しかしながら、我々は極域におけるこのような極端に微弱な降水量を計測する方法を構築できていない。論文は陸別町におけるシーロメーター、ディストロメーター、重量式降水量計測が微弱な降水をどのように検出するのかを調べた。降水重量計測が降水を検出しなかった期間に、ディストロメーターやシーロメーターが微弱な降水を検出することが分かった。本研究は、このような微弱な降水を比較的降水強度の強いタイプ I の極端微弱降水 (EWP-I) と強度のより弱いタイプ II の極端微弱降水 (EWP-II) とに分けた。EWP-II は、ディストロメーターによる降水粒子の検出及びシーロメーターによる後方散乱強度の増加によって検知され、実際に降水粒子が撮影された。EWP-II は主に夜間に観測され、そこでは放射冷却にともなう地上気温の低下が引き起こす相対湿度の上昇が重要である。ディストロメーターは氷飽和の条件下でのみ降水粒子を検出し、シーロメーターは昼間に最高気温を記録した後の気温低下は始まった比較的直ぐに後方散乱の増加を観測した。ディストロメーターは粒径が 125 μm 以下の粒子を検出しないことから、シーロメーターはより小さな粒子の影響を捉えた可能性がある。このような更に弱い降水を EWP-III として分類できる。EWP-II と EWP-III の検出は、極域における晴天降水を含む極めて弱い降水の、少なくとも発生を記録することができることを示している。

Correspondence to: N. Hirasawa, hira.n@nipr.ac.jp

Copyright ©2025 The Okhotsk Sea & Polar Oceans Research Association. All rights reserved.